Purdue University
Purdue e-Pubs

International Refrigeration and Air Conditioning Conference

School of Mechanical Engineering

2012

Inverse Modeling to Simulate Fault Impacts for Vapor Compression Equipment Part 1: Component Modeling and Validation

Howard Cheung
cheung@purdue.edu

James E. Braun

Follow this and additional works at: http://docs.lib.purdue.edu/iracc

Cheung, Howard and Braun, James E., "Inverse Modeling to Simulate Fault Impacts for Vapor Compression Equipment Part 1: Component Modeling and Validation" (2012). *International Refrigeration and Air Conditioning Conference.* Paper 1166.
http://docs.lib.purdue.edu/iracc/1166

This document has been made available through Purdue e-Pubs, a service of the Purdue University Libraries. Please contact epubs@purdue.edu for additional information.
Complete proceedings may be acquired in print and on CD-ROM directly from the Ray W. Herrick Laboratories at https://engineering.purdue.edu/Herrick/Events/orderlit.html

Inverse Modeling to Simulate Fault Impacts for Vapor Compression Equipment Part 1: Component Modeling and Validation

Howard CHEUNG*, James E. BRAUN

Ray W. Herrick Laboratories, School of Mechanical Engineering, Purdue University
West Lafayette, Indiana, U.S.A
E-mail: cheung@purdue.edu and jbraun@purdue.edu

* Corresponding Author

ABSTRACT

With the emergence of fault detection and diagnostics tools for air conditioning systems in the market, a fair and reliable evaluator, which tests the tools with a large array of data points from a variety of conditions and types of units, is needed. However, the number of data points necessary for reliable evaluation is too large to be generated through physical experiments. Also, existing forward models are difficult to employ for this application because of the requirement to have knowledge of many difficult-to-obtain component parameters and because of very long computation times. To address the issue, a gray box modeling approach is being developed to account for the effects of both operating conditions and faults on performance. This gray-box approach uses experimental data and inverse modeling to determine the values of parameters for each component of a vapor compression cycle. This has led to a fast and robust component-based model that is trained with a limited set of experimental data from normal and faulted conditions, and a few readily available geometrical measurements. Existing component modeling approaches have been simplified to reduce the number of parameters and computational costs. During parameter training for each component, optimization of a cost function is carried out to minimize residuals between experiments and simulation. This paper presents the models, training approaches, and validation results for individual components for a 3-ton R410A packaged air conditioner. Component models constructed included compressor, condenser, evaporator, fixed orifice expansion device, and refrigerant pipes. A companion paper presents the system-level modeling and validation, along with models and results for simulation of faults.

1. INTRODUCTION

Fault detection and diagnostics (FDD) tools can identify faults in air conditioning systems and have become more available to the public in recent years. To assist consumers in evaluating available FDD products, a systematic evaluation scheme is needed. However, to avoid bias in the evaluation process, it is necessary to examine the FDD tools with a large number of conditions. Obtaining the faulted system information from experiments only is too expensive, and forward modeling of systems may require a multitude of difficult-to-obtain parameters from a variety of systems. Furthermore, detailed forward models can take a great deal of computation time. The current paper describes development of an approach in which inverse modeling is used to seek parameters for simplified models from experimental data of individual components under faulty conditions. It also facilitates the understanding of faulted operation and is able to simulate the system operation under unmeasured faulted conditions quickly and accurately.

The technique of parameter estimation for vapor compression cycle systems was described by Biegler and Tjoa (1993). Sequential quadratic programming was tested for estimating heat transfer conductances over a heat exchanger network. Rabehl et al. (1999) estimated parameters of a heat exchanger with water and 50% ethylene/glycol for heat transfer rate and pressure drop. Jin and Spitler (2002) used multi-variant optimization to estimate the parameters of a water-to-water heat pump model simulated with catalog data. Hariharan and Rasmussen (2010) presented a method to estimate parameters for thermostatic expansion valves and variable speed compressors for dynamic modeling. Zakula et al. (2011) modeled a variable speed system by estimating parameters of a compressor from experimental data.

In this paper, important components identified in Figure 1 are modeled with inverse modeling of the experimental data from a 3-ton R410A packaged unit with a fixed orifice expansion device, described in Shen (2006). The data include both non-faulted and faulted operation, including heat exchanger fouling and non-standard refrigerant charging. Refrigerant properties in the calculations were obtained from REFPROP version 8.0 (Lemmon, 2009).

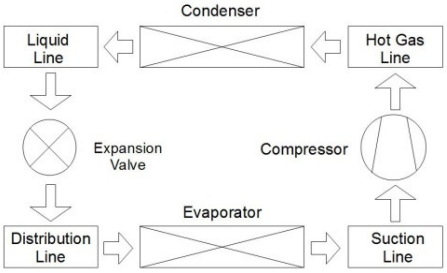

Figure 1: Component schematic of the model.

2. COMPONENT MODELS

2.1 Compressor model

The compressor model employed in the current study is based on a semi-empirical model of Jähnig et al. (2000) that was simplified to form a 4-parameter model as shown in Eqs. (1), (2) and (3), where inlet density is obtained by assuming thermodynamic equilibrium at the inlet.

$$\dot{m}_r = \rho_{comp,in}\left(C_0 + C_1\left(\frac{P_{comp,out}}{P_{comp,in}}\right)^{\frac{1}{q}}\right) \tag{1}$$

$$\begin{aligned} \dot{W}_{comp} f(P_{comp,in}, P_{comp.out}) = &\quad \dot{m}_r \frac{q}{q-1}\frac{P_{comp,in}}{\rho_{comp,in}}\left(\left(\frac{P_{comp,out}}{P_{comp,in}}\right)^{1-\frac{1}{q}} - 1\right) \\ f(P_{comp,in}, P_{comp.out}) = &\quad C_2 + C_3 P_{comp,in} + C_4 P_{comp,out} \\ &+ C_5 P_{comp,in}^2 + C_6 P_{comp,in} P_{comp,out} + C_7 P_{comp,out}^2 \end{aligned} \tag{2}$$

$$hl_{comp} = 1 - \frac{\dot{m}_r (h_{r,comp,in} - h_{r,out})}{\dot{W}_{comp}} \tag{3}$$

2.2 Heat exchanger models

The condenser model was simplified from Bell (2010) by using a moving-boundary method at steady state. The heat exchanger is divided into sections according to the refrigerant phase, and each section is modeled with ε-NTU methods under a crossflow configuration. The details of the approach can be found in Bell (2010). The most important parameters to the heat transfer rate are given in Eqs. (4), (5), (6), (7), with reference to Figure 2. Equation (6) was derived from the Dittus-Boelter equation (Incropera et al., 2007). The pressure drop of the refrigerant across the condenser was modeled with Eq. (11), which was derived from considering the frictional and acceleration components of pressure drop (Wallis, 1969), where the two-phase average density is estimated by Eqs. (8), (9) and (10), and the densities at the inlet and outlet are estimated by the Zivi (1964) model if the refrigerant is two-phase.

$$\frac{1}{UA_{overall,cond,sec}} = \frac{1}{U_{a,cond} A_{cond,rated}} + \frac{1}{U_{r,cond,sec} A_{cond,rated}} \tag{4}$$

$$U_{a,cond} = U_{a,rated,cond}\left(\frac{\dot{m}_a}{\dot{m}_{a,cond,rated}}\right)^{n_{cond}} \tag{5}$$

$$U_{r,cond,1\phi} = U_{r,cond,rated,1\phi} \frac{\left(\frac{\dot{m}_r}{\mu_{r,1\phi}}\right)^{0.8}\left(\frac{\mu_{r,1\phi} c_{p,r,1\phi}}{k_{r,1\phi}}\right)^{0.4} k_{r,1\phi}}{K_{rated,cond,1\phi}} \tag{6}$$

$$U_{r,cond,tp} = U_{r,cond,tp,rated}\frac{\dot{m}_r}{\dot{m}_{r,rated}} \tag{7}$$

$$\rho_{r,tp} = \rho_{r,v}\alpha_r + \rho_{r,l}(1-\alpha_r) \tag{8}$$

$$\alpha_r = \begin{cases} 1 & \text{if } x_{r,min} = 1 \\ 0 & \text{if } x_{r,max} = 0 \\ -\frac{C_{tp}(ln(\frac{C_{tp}(x_{r,max}-1)-x_{r,max}}{C_{tp}(x_{r,min}-1)-x_{r,min}})+x_{r,max}-x_{r,min})-x_{r,max}+x_{r,min}}{(x_{r,max}-x_{r,min})(C_{tp}-1)^2} & \text{otherwise} \end{cases} \tag{9}$$

$$C_{tp} = \left(\frac{\rho_{r,v}}{\rho_{r,l}}\right)^{\frac{2}{3}} \tag{10}$$

$$\begin{aligned} & P_{r,cond,in} - P_{r,cond,out} \\ = \; & C_1 w_{sh}\frac{(\dot{m}_r/\dot{m}_{r,rated,cond})^2}{\rho_{r,v}/\rho_{r,v,rated,cond}} + C_2 w_{tp}\frac{(\dot{m}_r/\dot{m}_{r,rated,cond})^2}{\rho_{r,tp}/\rho_{r,rated,cond}}\left(\frac{\mu_{r,v}}{\mu_{r,v,rated,cond}}\right)^{C_3} \\ + \; & C_4 w_{sc}\frac{(\dot{m}_r/\dot{m}_{r,rated,cond})^2}{\rho_{r,l}/\rho_{r,out,rated,cond}} + C_5\dot{m}_r^2\rho_{r,rated,cond}\left(\frac{1}{\rho_{r,cond,out}} - \frac{1}{\rho_{r,cond,in}}\right) \end{aligned} \tag{11}$$

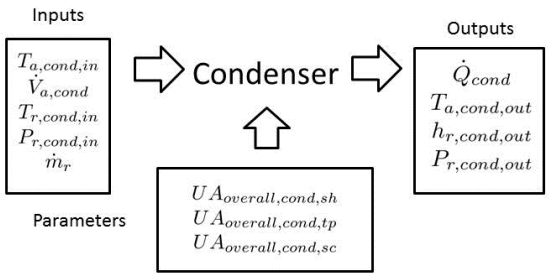

Figure 2: Condenser model schematic.

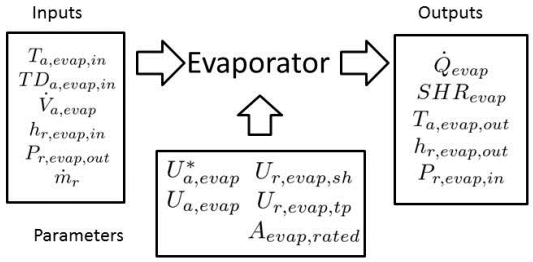

Figure 3: Evaporator model schematic.

The evaporator model depicted in Figure 3 is similar to the condenser model, but with the addition of the partial-wet-partial-dry scheme of Braun (1989) for each section corresponding to a refrigerant phase. The outlet refrigerant pressure of the evaporator was used as an input instead of the inlet pressure, as shown in Figure 3, to ensure that the surface temperature of the coil can be captured reasonably in the moving boundary method calculation. The relationship between the parameters and the heat transfer conductances of the model are shown in Eqs. (12), (13) and (14). The area ratios were computed in the model during the solution processes.

$$UA_{a,evap,sec} = w_{sec,evap}U_{a,evap}A_{evap,rated} \tag{12}$$

$$UA^*_{a,evap,sec} = w_{sec,evap}U^*_{a,evap}A_{evap,rated} \tag{13}$$

$$UA_{r,evap,sec} = w_{sec,evap}U_{r,evap,sec}A_{evap,rated} \tag{14}$$

The heat transfer coefficients in Eqs. (12), (13) and (14) were obtained by Eqs. (15) to (19) which were derived from fin correlations in McQuiston and Parker (1988) and heat transfer correlations in Shah (1982), where calculation of Ψ(x) can be found. The heat transfer coefficient for the superheated section can be calculated from Eq. (6), with all parameters obtained from the evaporator performance data. The pressure drop across the evaporator was obtained by considering the frictional and accelerational components of the pressure drop (Wallis, 1969) as in Eq. (20).

$$U_{a,evap} = U_{a,rated,evap}\left(\frac{\dot{m}_a}{\dot{m}_{a,evap,rated}}\right)^{n_{evap}}\frac{tanh(p_{evap})}{p_{evap}} \tag{15}$$

$$U^*_{a,evap} = U_{a,rated,evap}\left(\frac{\dot{m}_a}{\dot{m}_{a,rated}}\right)^{n_{evap}} \frac{tanh(K_a)}{K_a} \frac{1}{c_{p,a}} \tag{16}$$

$$K_a = \left(U_{a,rated,evap}\left(\frac{\dot{m}_a}{\dot{m}_{a,rated,evap}}\right)^{n_{evap}} \frac{c_s}{c_{p,a}}\right)^{1/2} p_{evap} \tag{17}$$

$$c_s = \frac{dh_{a,sat}}{dT}\Big|_{T=T(P=P_{r,evap,out},x_r=1)} \tag{18}$$

$$U_{r,evap,tp} = U_{r,evap,tp,rated}\left(\frac{\dot{m}_r}{\rho_{r,l}\mu_{r,l}}\right)^{0.8}\left(\frac{\rho_{r,l}c_{p,r,l}}{k_{r,l}}\right)^{0.4} k_l \int_{x_{r,in}}^{x_{r,out}} \psi_i(x_r)(1-x_r)^{0.8} dx_r \tag{19}$$

$$\begin{aligned} & P_{r,evap,in} - P_{r,evap,out} \\ = \;& C_1 w_{tp} \frac{(\dot{m}_r/\dot{m}_{r,rated,evap})^2}{\rho_{r,tp}/\rho_{r,rated,evap}} \left(\frac{x_{r,in}\mu_{r,v}/\rho_{r,v} + (1-x_{r,in})\mu_{r,l}/\rho_{r,l}}{x_{r,in}/\rho_{r,v} + (1-x_{r,in})/\rho_{r,l}} \frac{1}{\mu_{r,v,rated,evap}}\right)^{C_4} \\ + \;& C_2 w_{sh} \frac{(\dot{m}_r/\dot{m}_{r,rated,evap})^2}{\rho_{r,v}/\rho_{r,out,rated,evap}} \\ + \;& C_3 \left(\frac{\dot{m}_r}{\dot{m}_{r,rated,evap}}\right)^2 \rho_{r,rated}\left(\frac{1}{\rho_{r,out,evap}} - \frac{1}{\rho_{r,in,evap}}\right) \end{aligned} \tag{20}$$

2.3 Expansion Valve model

The expansion valve model simulates the behavior of a fixed orifice. It was derived from Payne and O'Neal (1999). The diameter and the length of the fixed orifice model were estimated from the experimental data. The expansion process was assumed to be adiabatic. The resultant model is described in Figure 4.

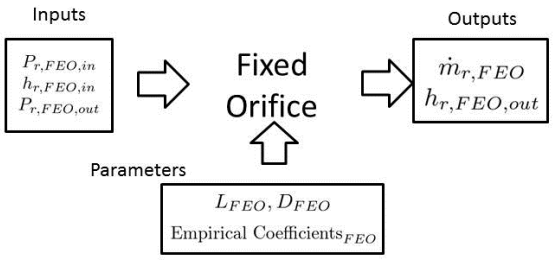

Figure 4: Expansion valve model schematic.

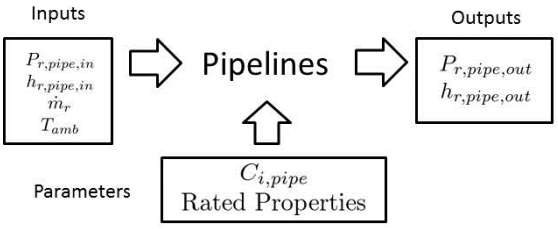

Figure 5: Pipeline model schematic.

2.4 Pipeline model

The pipeline model simulates pressure drop and enthalpy change of the refrigerant passing through the refrigerant pipes, as illustrated in Figure 5. Coefficients in Eqs. (21) and (22) were estimated from data to describe pressure drop and enthalpy change along the refrigerant pipes. Eq. (21) was constructed by estimating the frictional and accelerational pressure drop, and Eq. (22) was used to estimate the heat transfer as a consequence of the air-side natural convection from the refrigerant pipe to the ambient.

$$\begin{aligned} P_{r,pipe,in} - P_{r,pipe,out} = \;& C_1\left(\frac{\dot{m}_r}{\dot{m}_{r,pipe,rated}}\right)^{C_2}\left(\frac{\mu_{r,in}}{\mu_{r,pipe,rated}}\right)^{C_3}\left(\frac{\rho_{r,in}}{\rho_{r,pipe,rated}}\right)^{C_4} \\ & + C_5\left(\frac{\dot{m}_r}{\dot{m}_{r,pipe,rated}}\right)^2 \rho_{r,pipe,rated}\left(\frac{1}{\rho_{r,pipe,out}} - \frac{1}{\rho_{r,pipe,in}}\right) \end{aligned} \tag{21}$$

$$\begin{aligned} & \frac{\dot{m}_{r,pipe}}{\dot{m}_{r,pipe,rated}} \frac{h_{r,pipe,in} - h_{r,pipe,out}}{\Delta h_{r,pipe,rated}} \\ = \;& \left(\frac{1}{C_6\left|\frac{T_{r,pipe,in} - T_{amb}}{T_{amb}}\right|^{C_7}} + \frac{\dot{m}_{r,pipe,rated}^{C_9}}{C_8 \dot{m}_r^{C_9}}\right)^{-1} \frac{T_{r,pipe,in} - T_{amb}}{\Delta T_{pipe,rated}} \end{aligned} \tag{22}$$

3. COMPONENT PARAMETER ESTIMATION

Parameters of different component models are estimated by minimizing cost functions using least squares methods. In some cases, constraints are applied to avoid unphysical parameters. For example, Shah (1982) is used to calculate a maximum value for the rated refrigerant-side heat transfer coefficient. Compressor parameters are estimated by minimizing the sum squared differences between measurement and prediction for mass flow rate, power consumption and refrigerant enthalpy gain across the compressor. Condenser parameters are obtained by minimizing the sum squared differences between the measured and predicted heat transfer rate and pressure drop. The sum of squares of the differences between the measured and predicted mass flow rate are also minimized to estimate the geometry of the fixed orifice model. Minimizations of the sum of squares of the differences between measured and predicted refrigerant enthalpy change and pressure drops are also conducted with refrigerant pipe data to quantify the pipe parameters.

Since the evaporator model estimates both the heat transfer rate and the humidity removal capability accurately, a cost function Eq. (23) was designed to find the set of parameters necessary to minimize the difference between the estimation and the measurement of both variables.

$$J = \sqrt{\Sigma \frac{1}{N}\left(\frac{\hat{\dot{Q}}_{r,evap} - \dot{Q}_{r,evap}}{\dot{Q}_{r,evap}}\right)^2}\left(1 + 100\sqrt{\Sigma \frac{1}{N}\left(\frac{\hat{SHR}_{evap} - SHR_{evap}}{SHR_{evap}}\right)^2}\right) \tag{23}$$

4. RESULTS AND DISCUSSIONS

Since a Coriolis mass flow meter is not accurate with two-phase inlet conditions, only data with subcooling at the expansion valve inlet (the location of the mass flow meter) greater than 3K were used to estimate the parameters. In addition, when estimating the compressor performance, only data with inlet superheat greater than 1K were used to avoid potential two-phase fluid at the inlet and error in enthalpy calculation. Likewise, the same superheat requirement was imposed on the evaporator outlet condition for the same reason. All coefficients estimated are listed in the appendix.

4.1 Compressor

The results of the compressor estimation are compared with measured values in Figure 6, Figure 7 and Figure 8. The coefficients of determination for the results in Figure 6, Figure 7 and Figure 8 are 0.9525, 0.9958 and 0.9139, indicating good agreement between model and measurements, despite one outlier in Figure 8.

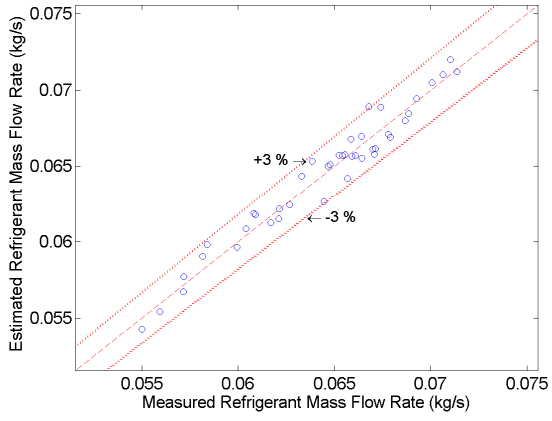

Figure 6: Accuracy of compressor refrigerant mass flow rate model.

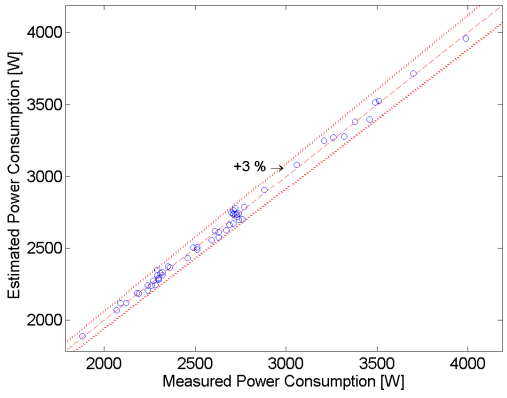

Figure 7: Accuracy of compressor power consumption model.

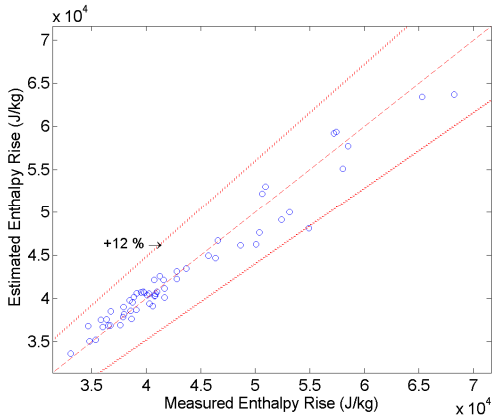

Figure 8: Comparisons of enthalpy change across the compressor.

4.2 Heat Transfer Rates and Sensible Heat Ratios

The results of the heat transfer rate and sensible heat ratio estimation are shown from Figure 9 to Figure 13. Only one measurement station was available between evaporator and expansion valve in this data set so the distribution line in Figure 1 was not modeled due to insufficient data at the inlet and outlet of the distribution line.

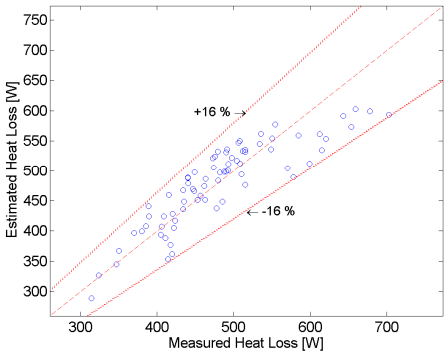

Figure 9: Comparisons of heat loss across the compressor discharge gas line.

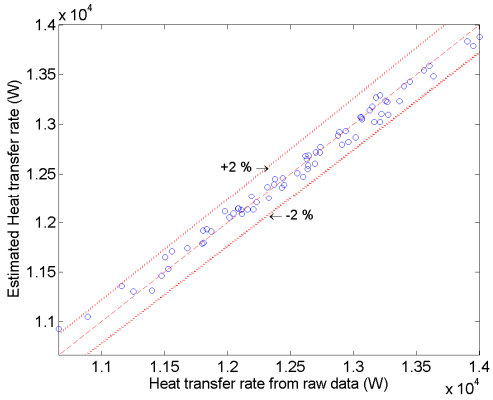

Figure 10: Comparisons of heat transfer rate of the condenser.

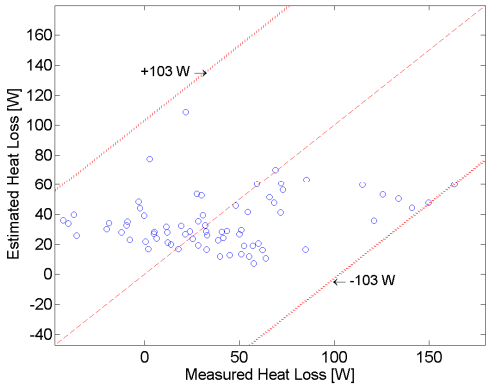

Figure 11: Comparisons of heat loss across the liquid line.

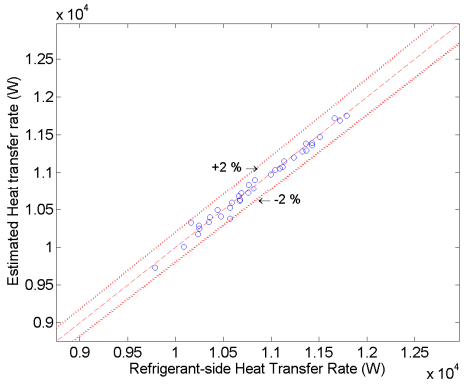

Figure 12: Comparisons of heat transfer rate of the evaporator.

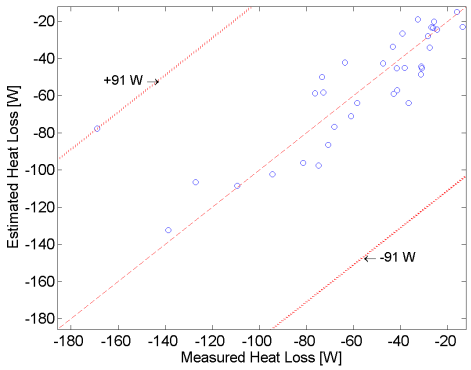

Figure 13: Comparisons of heat loss across the compressor suction line.

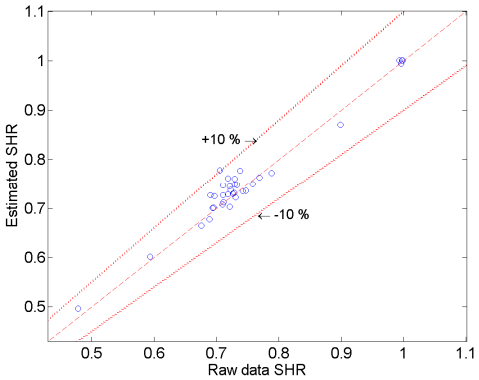

Figure 14: Comparisons of sensible heat ratio of the evaporator.

While Figure 10, Figure 12 and Figure 14 show that the heat transfer rates and sensible heat ratio are estimated with accuracy within 2%, 2% and 10% respectively, the heat loss rates in Figure 9, Figure 11 and Figure 13 across the pipelines show poor accuracy. This is assumed to be a result of the unavailability of the surrounding air temperatures around the pipelines, which were consequently approximated with the ambient air temperature. The air temperatures around the pipelines, because of their location inside the packaged unit, might be different from the ambient air temperatures and created the deviation. However, the magnitudes of the heat transfer rates across the piping are relatively small compared to the condenser and evaporator heat transfer rates so the errors are less important.

4.3 Expansion Valve

Mass flow rate comparisons for the fixed orifice model are plotted in Figure 15. The predictions are within 2% deviation, indicating very close agreement.

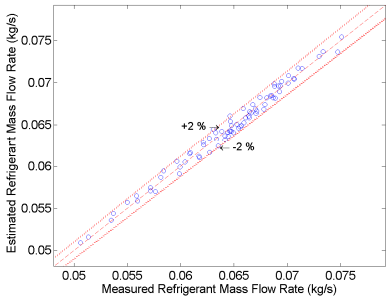

Figure 15: Comparisons of mass flow rate across the expansion valve.

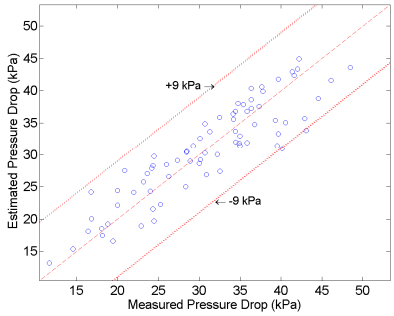

Figure 16: Comparisons of pressure drop across the compressor discharge line.

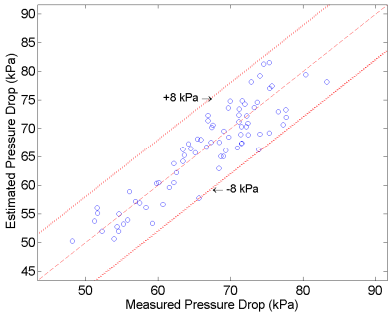

Figure 17: Comparisons of pressure drop across the condenser.

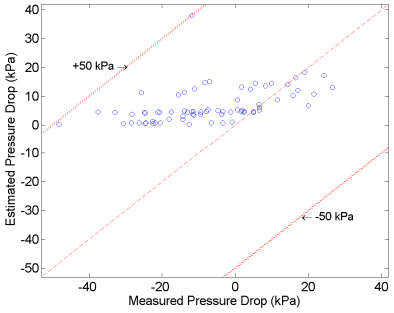

Figure 18: Comparisons of pressure drop across the liquid line.

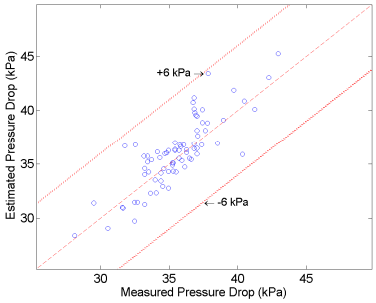

Figure 19: Comparisons of pressure drop across the evaporator.

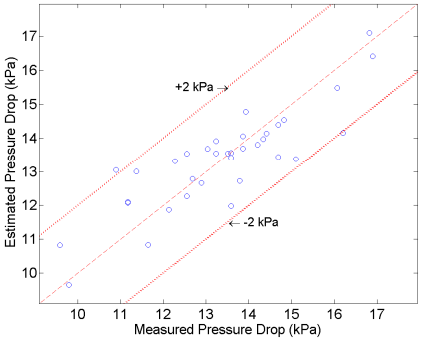

Figure 20: Comparisons of pressure drop across the compressor suction line.

4.4 Pressure drop

The estimated pressure drop across the heat exchangers and pipelines are shown from Figure 16 to Figure 20. Figure 18 shows a much larger deviation in pressure drop than the other components. It was found that a majority of the liquid line data exhibits a pressure increase, which is physically impossible. The model in Eq. (21) is restricted to output positive pressure drop values only. This creates a very large deviation when the data show a large negative pressure drop and the model can only provide a positive value.

4. CONCLUSIONS

In this paper, semi-empirical models were introduced to simulate the heat transfer, pressure drop and power consumption characteristics of the major components of a vapor compression cycle. Experimental data from a packaged unit were used to demonstrate the parameter estimation process and the accuracy and the reliability of the model. Discrepancies between some estimation results and the measurements exist in the pipeline models, but the magnitudes of the errors are negligible compared to major cycle components. The component models can be combined together to simulate the complete cycle operation, which is described in a companion paper (Cheung and Braun, 2012). In the future, the modeling approach will be used with experimental data from other units and will be modified to include other significant factors.

NOMENCLATURE

A	area	(m^2)	**Subscripts**	
α	average void fraction	(--)	1ϕ	single phase
C, n, p	coefficients	(varies)	a	air
c_p	specific heat capacity at constant pressure	(J/kg-K)	comp	compressor
c_s	analogous specific heat for air-water mixture	(J/kg-K)	cond	condenser
D	diameter	(m)	evap	evaporator
h	enthalpy	(J/kg)	FEO	fixed orifice
hl	heat loss ratio	(--)	in	inlet
J	cost function	(--)	l	saturated liquid
K	tuning coefficients for heat transfer coefficients	(varies)	max	maximum
k	conductivity	(W/m-K)	min	minimum
L	length	(m)	pipe	pipeline
m	mass flow rate	(kg/s)	out	outlet
N	number of data points	(--)	overall	overall
P	pressure	(kPa)	r	refrigerant
Ψ	tuning coefficient from Shah (1982) correlation	(--)	rated	rated
Q	heat transfer rate	(W)	sc	subcooled
q	specific heat ratio	(--)	sec	refrigerant phase
ρ	density	(kg/m^3)	sh	superheated
SHR	sensible heat ratio	(--)	tp	two-phase
T	dry-bulb temperature	(K)	v	saturated vapor
TD	dewpoint temperature	(K)		

U	heat transfer coefficient	(W/m^2-K)	**Superscript**
U^*	heat and mass transfer coefficient	(kg/s)	^ estimated
V	airflow	(m^3/s)	
W	power consumption	(W)	
w	area ratio	(--)	
x	thermodynamic quality	(--)	

REFERENCE

Bell, I., 2010, ACHP [Software]. Available from http://achp.sourceforge.net/

Biegler, L. T., Tjoa, I., 1993, "A parallel implementation of parameter estimation with implicit models", *Annals of Operations Research*, 42: 1 - 23

Braun, J. E., 1989, *Methodologies for the Design and Control of Central Cooling Plants*, Ph.D. Thesis, University of Wisconsin – Madison, WI

Cheung, H., Braun, J. E., 2012, "Inverse Modeling to Simulate Fault Impacts for Vapor Compression Equipment Part 2: System Modeling and Validation", *Proceedings of the 14th International Refrigeration and Air Conditioning Conference at Purdue*, West Lafayette, IN

Hariharan, N., Rasmussen, B. P., 2010, "Parameter Estimation for Dynamic HVAC Models with Limited Sensor Information", *Proceedings of 2010 American Control Conference*. Baltimore, MD

Incropera, F. P., DeWitt, D. P., Bergman, T. L., Lavine, A. S., 2007, *Fundamentals of Heat and Mass Transfer*, New York, NY: John Wiley & Sons

Jähnig, D. I., Reindl, D. T., Klein S. A., 2000, "A Semi-Empirical Method for Representing Domestic Refrigerator/Freezer Compressor Calorimeter Test Data", *ASHRAE Transactions*, 106 (2): 122 – 130

Jin, H. and Spitler J. D., 2002, "A Parameter Estimation Based Model of Water-to-Water Heat Pumps for Use in Energy Calculation Program", *ASHRAE Transactions*, 108 (1): 3 – 17

Lemmon, E.W., Huber, M.L., McLinden, M.O., 2009, *NIST Standard Reference Database 23: Reference Fluid Thermodynamic and Transport Properties-REFPROP, Version 8.0, Standard Reference Data Program*, Gaithersburg, MD: National Institute of Standards and Technology

Lockhart, R. W., Martinelli, R. C., 1949, "Proposed Correlation of Data for Isothermal Two-Phase Two-component Flow in Pipes", *Chemical Engineering Progress*, 45: 39 – 48

McQuiston, F. C., Parker, J. D., 1988, *Heating, Ventilating, and Air Conditioning – Analysis and Design*, New York, NY: John Wiley & Sons

Payne, W. V, O'Neal, D. L., 1999, "Multiphase Flow of Refrigerant R410A Through Short Tube Orifices", *ASHRAE Transactions*, 105 (2): 66 – 74

Rabehl, R. J., Mitchell, J. W., Beckman, W. A., 1999, "Parameter Estimation and the Use of Catalog Data in Modeling Heat Exchangers and Coils", *HVAC&R Research*, 5 (1): 3 – 17

Shah, M. M., 1982, "Chart Correlation for Saturated Boiling Heat Transfer: Equations and Further Study", *ASHRAE Transactions*, 88 (1): 165 – 192

Shen, B., 2006, *Improvement and validation of unitary air conditioner and heat pump simulation models at off-design conditions*, Ph.D. thesis, Ray W. Herrick Laboratories, Purdue University, Ind. Report No. 6304-1 HL2006-1

Wallis, G. B., 1969, *One-dimensional Two-phase Flow*, New York, NY: McGraw -Hill

Zakula, T., Gayeski, N. T., Armstrong, P. R., Norford L. K., 2011, "Variable-speed Heat Pump Model for a Wide Range of Cooling Conditions and Loads", *HVAC&R Research*, 17 (5): 670 – 691

Zivi, S. M., 1964, "Estimation of steady-state steam void-fraction by means of the principle of minimum entropy production", *Journal of Heat Transfer*, 86: 247 – 252

ACKNOWLEDGEMENT

The authors acknowledge National Institute of Standards and Technology (NIST) Grant # 104867 for sponsoring the project development. The authors would also like to acknowledge David Yuill from Purdue University and Drs. Vance Payne and Piotr Domanski from NIST for their help on this project.

APPENDIX

Table A.1: Coefficients in Equations.

Hot Gas Line		Liquid Line		Suction Line		Expansion Valve	
C_1 [kPa]	6.829E+01	C_1 [kPa]	4.446E+00	C_1 [kPa]	7.749E+00	D [m]	1.750E-03
C_2	1.518E+00	C_2	2.426E-01	C_2	2.912E-01	L [m]	1.321E-02
C_3	1.852E+00	C_3	1.010E+01	C_3	1.398E+01		
C_4	-2.185E-01	C_4	0.000E+00	C_4	-2.779E-01		
C_5 [kPa]	1.271E+03	C_5 [kPa]	0.000E+00	C_5 [kPa]	2.611E+02		
C_6	1.557E-02	C_6	1.004E+00	C_6	2.283E+01		
C_7	-2.913E+00	C_7	-2.366E+02	C_7	1.675E+00		
C_8	1.361E+00	C_8	8.159E+00	C_8	1.826E+03		
C_9	2.428E+00	C_9	7.593E+00	C_9	6.376E+01		
ΔT_{rated} [K]	4.024E+01	ΔT_{rated} [K]	5.194E+00	ΔT_{rated} [K]	-3.019E+01		
Δh_{rated} [J/kg]	6.313E+03	Δh_{rated} [J/kg]	3.328E+01	Δh_{rated} [J/kg]	-2.737E+03		
$m_{r,rated}$ [kg/s]	6.171E-02	$m_{r,rated}$ [kg/s]	6.171E-02	$m_{r,rated}$ [kg/s]	6.170E-02		
μ_{rated} [kg/m-s]	1.668E-05	μ_{rated} [kg/m-s]	9.600E-05	μ_{rated} [kg/m-s]	1.304E-05		
ρ_{rated} [kg/m3]	1.005E+02	ρ_{rated} [kg/m3]	9.733E+02	ρ_{rated} [kg/m3]	3.857E+01		

Condenser		Evaporator		Compressor	
n_{cond}	3.028E+00	$U_{a,rated,evap}$ [W/K]	7.769E+02	C_0 [/s]	2.090E-03
$U_{a,rated,cond}$ [W/K]	9.492E+03	p_{evap}	7.882E-08	C_1 [/s]	-1.980E-04
$U_{r,cond,rated,sh}/K_{rated,cond,sh}$ [K/m$^{0.8}$]	5.004E-01	n_{evap}	8.400E-01	C_2	5.409E-01
$U_{r,cond,rated,sc}/K_{rated,cond,sc}$ [K/m$^{0.8}$]	1.517E+00	$m_{a,rated,evap}$ [kg/s]	6.581E-01	C_3 [/kPa]	4.834E-04
$U_{r,cond,tp,rated}$ [W/K]	1.533E+04	$U_{r,evap,rated,sh}/K_{rated,evap,sh}$ [K/m$^{0.8}$]	1.364E+00	C_4 [/kPa]	-8.941E-05
$m_{a,rated}$ [kg/s]	1.242E+00	$U_{r,evap,tp,rated}$ [K/m$^{0.8}$]	1.661E+01	C_5 [/kPa2]	-5.876E-07
$m_{r,rated}$ [kg/s]	6.171E-02	$m_{r,rated}$ [kg/s]	6.170E-02	C_6 [/kPa2]	3.584E-07
C_1 [kPa]	1.715E+02	C_1 [kPa]	1.444E+01	C_7 [/kPa2]	-5.392E-08
C_2 [kPa]	1.655E+02	C_2 [kPa]	7.637E+00	hl_{comp}	3.670E-02
C_3	-4.791E+00	C_3 [kPa]	4.119E+00		
C_4 [kPa]	1.705E+01	C_4	-3.621E+00		
C_5 [kPa]	0.000E+00	$A_{cond,rated}$ [m^2]	1.484E+00		
$A_{cond,rated}$ [m^2]	1.484E+00	$\mu_{v,rated}$ [kg/m-s]	1.270E-05		
$\mu_{v,rated}$ [kg/m-s]	1.589E-05	ρ_{rated} [kg/m^3]	3.144E+02		
ρ_{rated} [kg/m^3]	1.034E+02	$\rho_{out,rated}$ [kg/m^3]	3.942E+01		
$\rho_{out,rated}$ [kg/m^3]	9.713E+02				